Coherence Estimation of Widely Demanded AW3D30 and SRTM 1-Arcsecond Space-Borne Global DEMs

Umut Gunes SEFERCIK (1), Umit GOKMEN (2), Can ATALAY (1)

[1] Dept. of Geomatics Engineering, Zonguldak Bülent Ecevit Uni., 67100, Zonguldak, Turkey
[2] Graduate School of Natural and Applied Sciences, Zonguldak Bülent Ecevit Uni., 67100, Zonguldak, Turkey
E-mail: sefercik@beun.edu.tr; canatalay@beun.edu.tr; umtgokmen@yahoo.com.tr

ABSTRACT: Global digital elevation models (GDEMs), the three dimensional digital cartographic representation of the Earth topography, have a crucial impact on many geo-spatial analyses. In these days, recently released ALOS World 3D 30 m (AW3D30) and 1 arc-second (~30 m) Shuttle Radar Topography Mission (SRTM) C-band GDEMs are very popular and widely in demand by scientific community. In this paper, we comprehensively analysed the coherence level of these GDEMs in country-scale calculating and interpreting the influence of terrain inclination and land cover classes. The coherence between two GDEMs was estimated by model to model accuracy analysis and height-scaled colourful coherence map based on differential of GDEMs. The results demonstrated the significance of ascending and descending orbits, terrain inclination and land cover on the coherence level of AW3D30 and SRTM GDEMs clearly.

KEYWORDS: AW3D30, SRTM, GDEM, Coherence, Coherence map

1. Introduction

The three-dimensional (3D) Earth topography is presented by global digital elevation models (GDEMs) which can be generated by optical or radar space-borne remotely sensed data. The GDEMs are fundamental for many geo-spatial analyses such as mapping, 3D city planning, forestry, disaster monitoring and management, agriculture, as well as Earth sciences. Moreover, GDEMs make possible to work on countries and continents and used in wide range of applications (Carvalho et al. 2010; Bullard et al. 2011; DeLong et al. 2012; Heckmann et al. 2012; Schneider et al. 2012; Sefercik et al. 2018). Space-borne GDEMs are derived by two main techniques as optical stereoscopy (Li et al. 2002; Cuartero et al. 2005; Toutin 2008; Radhadevi et al. 2010; Hobi and Ginzler 2012) and interferometric synthetic aperture radar (InSAR) (Soergel et al. 2009; Sefercik and Soergel 2010).

The main goal of this paper is to demonstrate the coherence level between Advanced Land Observing Satellite (ALOS) World 3D 30m (AW3D30) and 1 arc-second Shuttle Radar Topography Mission (SRTM) C-band, recently released optical stereoscopic and InSAR GDEMs by Japan Aerospace Exploration Agency (JAXA) and US National Aeronautics Space Administration (NASA). Although analysed GDEMs are much in demand by scientific community, there is a lack about their discontinuities in the literature. In fact, they have several dissimilarities depending on different imaging geometries and sensor characteristics. To show the coherence level of the GDEMs in different land cover classes and inclined terrain, Turkey was preferred as a convenient study area with its mountainous and multi-class topography. Turkey is located on four Universal Transverse Mercator (UTM) zones as 35-38 that's why mosaics of the GDEMs were produced by completing required transformations in these zones. By comprehensive visual and statistical analysis, considerable discontinuities were determined and interpreted.

The paper was organized as follows: an information about the study area is given in section 2. Imaging geometries of ALOS and SRTM missions are presented in section 3. The methodology workflow is presented in section 4. Results are given in section 5 followed by the conclusions.

2. Study area: TURKEY

Turkey is a transcontinental country in Eurasia covering 780.000 km^2 area. The topographic conditions of the country are mostly mountainous and hilly and land cover type is mainly forest. The orthometric elevation reaches up to 5137 m in Ararat Mountain. This kind of topographies are trigger for occurring space-borne remote sensing imaging problems and negatively influence the achieved data quality. On the other hand, open and flat areas are mostly misleading to interpret the performance of the remote sensing products. At this point of view, the study area is appropriate for the aims of this study. Figure 1 illustrates the study area and covering Universal Transverse Mercator (UTM) zones.

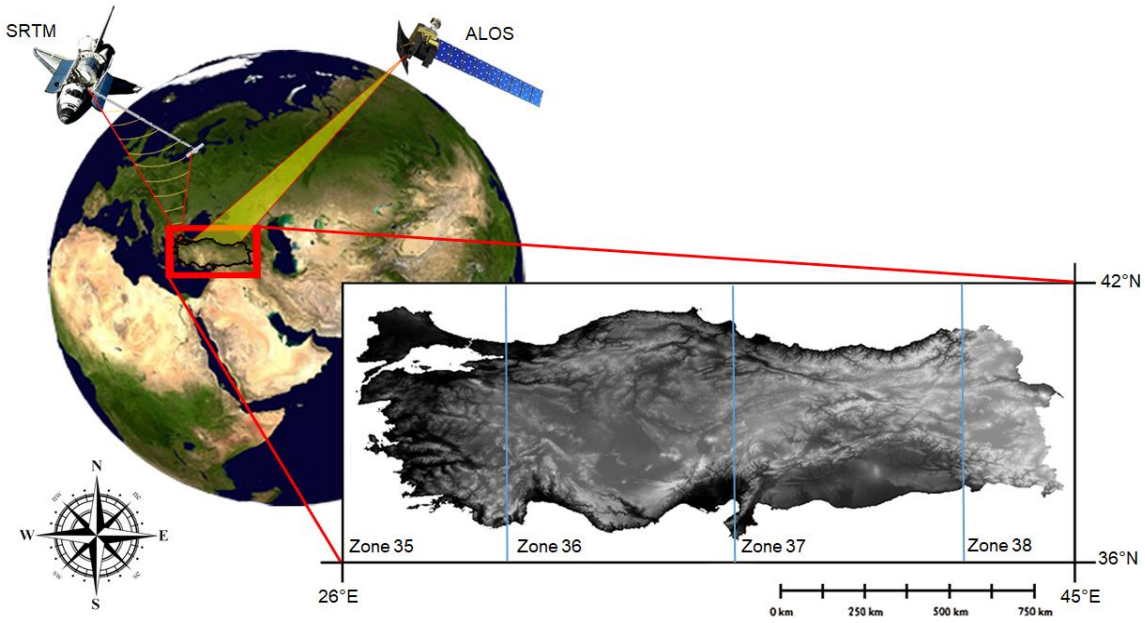

Figure 1. The study area and covering UTM zones (35-38)

3. Imaging geometries of the satellites

The imaging geometries and the characteristics of ALOS and SRTM 1-arcsecond GDEMs are presented in Figure 2 and Table 1. Where SRTM uses two antennas at different locations to measure the difference in range to the surface in single-pass, PRISM has three independent telescopes for nadir (70 km swath), forward and backward (35 km swath per each) views for the acquisition of stereo images.

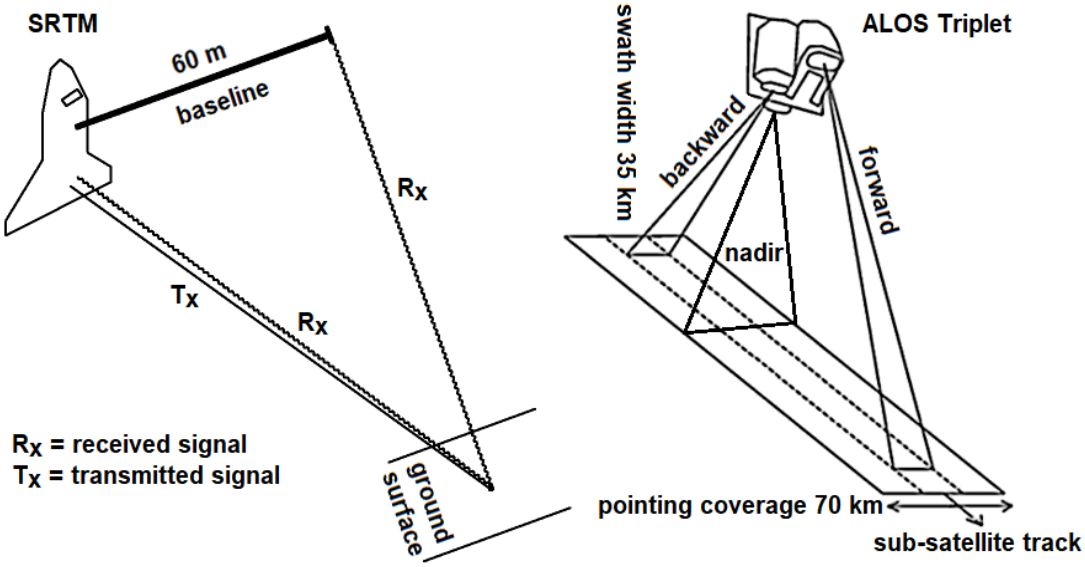

Figure 2. SRTM and ALOS Prism imaging geometries

2

Table 1. Specifications of the missions and GDEMs

Specification	Mission	
	SRTM	ALOS
Made in	USA/Germany	Japan
Launch date	11.02.2000	24.01.2006
Sensor/band	C-band	Prism
Spatial resolution of images	20 m×30 m (Az×Rg)	2.5 m
GDEM resolution	1 arc-second (~27m)	1 arc-second (~27m)
Coverage	Global (except pole zones)	Global (except pole zones)
Datum	UTM WGS84	UTM WGS84
Raw data acquisition date	2000	2006-2011
Version and version date	V4/2015	1.1/2017

4. Methodology

The utilized processing steps are presented in Figure 3. On Turkey, 48 tiles were determined for easy data processing and the outcomes of the tiles were combined. The area was classified as open areas, forest, water and inclined areas (Figure 4) and the coherence analysis were completed for each. The classification was realized utilizing highly accurate raster Country maps. The geolocation accuracies of the maps were tested by matching coastal lines.

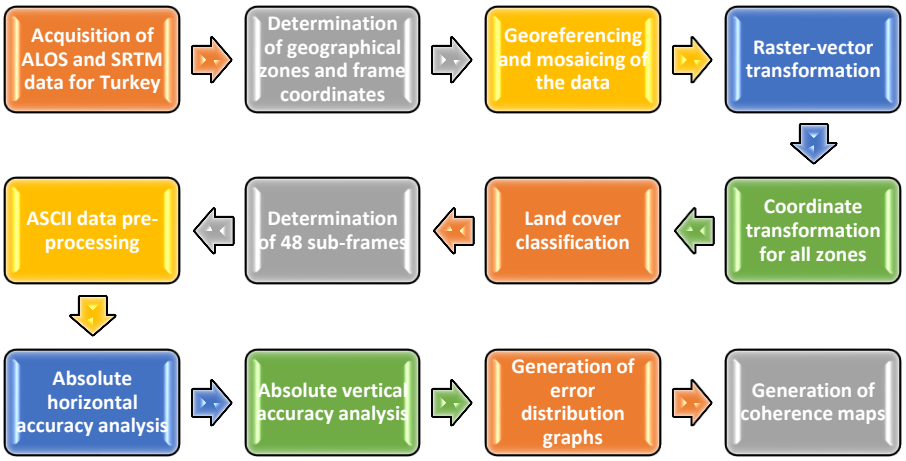

Figure 3. Methodology workflow

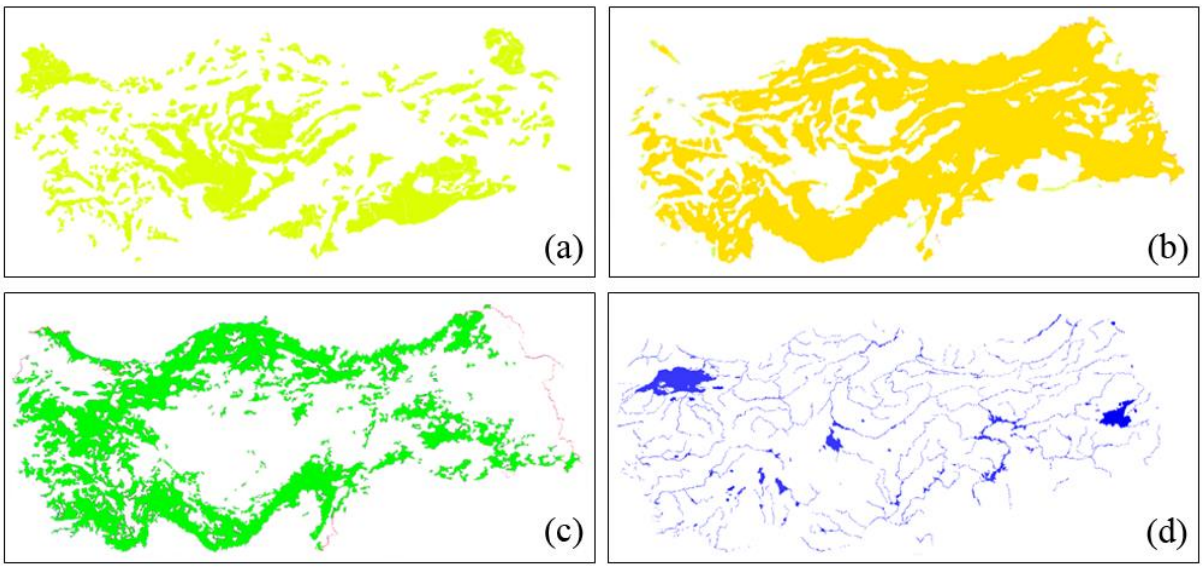

Figure 4. Land cover classes and inclined terrain: (a) open and uninclined, (b) inclined areas, (c) forest, (d) water

3

For analysing the coherence of AW3D30 and SRTM, some pre-processing steps were applied. First, the vertical datum and the coordinate systems of GDEMs were fixed. The common coordinate system and the datum were used as Universal Transverse Mercator (UTM) and World Geodetic System 1984 (WGS84), and the geoid undulations were calculated based on orthometric heights. The main rule of a correct vertical accuracy assessment is 100% horizontal overlap of compared DEMs that's why the horizontal offsets between the GDEMs were eliminated by area based cross correlation (Baltsavias et al. 2008; Alobeid et al. 2010). Table 2 shows the estimated and eliminated horizontal geolocation errors in X and Y directions in each zone separately. As can be seen in Table 2, horizontal errors are around one pixel (30 m) in Y and one third of a pixel in X direction.

Table 2. Estimated and eliminated horizontal geolocation errors (μ is the average)

Master DEM	Slave DEM	Zone	ΔX (m)	ΔY (m)
SRTM (30m)	AW3D30 (30m)	35	30.44	-31.34
		36	10.30	-31.58
		37	3.64	-32.53
		38	2.75	-30.42
		μ	**11.78**	**-31.47**

In the analysis of coherence between GDEMs, standard deviation of height discrepancies (SZ) was used (equation 1). In addition to σ_Z, the normalized median absolute deviation (NMAD) of the pixel-based height differences between GDEMs was used as the second coherence indicator. In the case of normally distributed height discrepancies between compared DEMs, NMAD is identical to σ_Z. In abnormal distribution, the NMAD is bigger than σ_Z. Although a robust estimator, NMAD is not as sensitive in regard to σ_Z for the determination of minor outliers in a large data set (Hellerstein 2008).

NMAD is the derivative of median absolute deviation (MAD), which is a robust measure of the variability of a univariate sample of quantitative data. MAD and NMAD are calculated by equations 2 and 3, where $\widetilde{X}_j$ is the median of the univariate data set of height discrepancies (ΔZ_1, ΔZ_2, ..., ΔZ_n) and $\widetilde{X}_\iota$ is the median of height discrepancies from $\widetilde{X}_j$.

$$\sigma_Z = \sqrt{\frac{\sum_{i=1}^{n}(\Delta Z_i - \mu)^2}{n-1}} \quad (1)$$

$$MAD = \widetilde{X}_\iota\left[\left|\Delta Z_i - \widetilde{X}_j(\Delta Z_j)\right|\right] \quad (2)$$

$$NMAD = 1.4826 \times (MAD) \quad (3)$$

The coherence map of SRTM and AW3D30 was generated by equation 4. The height scale of the coherence map is between ±12 m because of being the maximum height difference between SRTM and AW3D30 after the elimination of systematic bias.

$$Coherence\ map = DiffDEM = GDEM_{SRTM} - GDEM_{AW3D30} \quad (4)$$

4

5. Results

Mosaicked SRTM and AW3D30 Turkey GDEMs are shown in Figure 5. The structures of the GDEMs look very similar and there is no any remarkable gap. In country scale, visual interpretation can only be possible for large height differences as more than a hundred meter that's why the numerical results are more meaningful for the interpretation of the coherence. Table 3 and 4 present the estimated absolute vertical geolocation errors between two GDEMs for used classes separately.

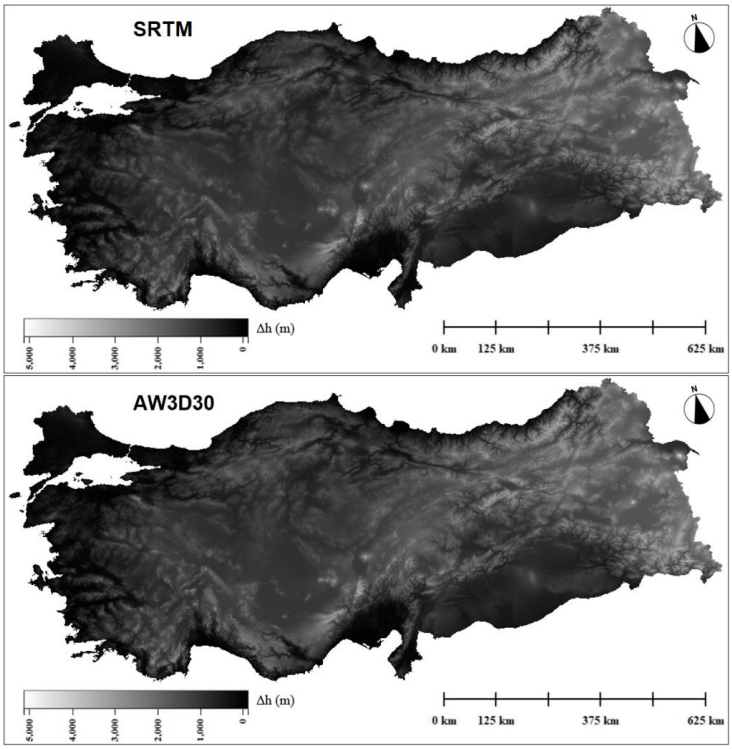

Figure 5. Mosaicked SRTM and AW3D30 DEMs

As shown in Table 3, in the open areas, the coherency is in the highest level and around 3.5 m as SZ and 2.5 m as NMAD. In the other land cover classes, the coherence decreases between 4 m and 4.5 m as SZ and 3 m and 3.5 m as NMAD. The results demonstrated that SRTM and AW3D30 GDEMs have difficulties to describe the non-open topographies. Nevertheless, entire height differences are under 5 m which indicates a well coherence between GDEMs.

As mentioned before, in Turkey, an inclined topography is dominant and the orthometric elevation reaches up to 5137 m. In Table 4, the considerable influence of terrain inclination is given by calculating the coherence in nearly flat areas (slope ≤ ~6°). In open and flat areas, the coherency arises to 2.6 m as SZ and 2.1 m as NMAD. In other land cover classes, the coherence is between 3 m and 4 m as SZ and 2.5 m and 3 m as NMAD. When, the results of inclined and uninclined areas are compared, the significant influence of terrain inclination is clearly demonstrated as ~1 m in SZ and ~0.5 m in NMAD.

Table 3. Estimated absolute vertical geolocation errors in land cover classes

Master DEM	Slave DEM	Land cover class	σ_Z (m)	NMAD (m)
SRTM (30m)	AW3D30 (30m)	Open	3.55	2.50
		Forest	4.62	3.18
		Water	4.07	2.50
		Inclined	4.39	3.06

5

Table 4. Effect of terrain inclination in land cover classes

Master DEM	Slave DEM	Land cover class	σ_Z (m) slope < $\tan^{-1}$ 0.1	NMAD (m) slope < $\tan^{-1}$ 0.1
SRTM (30m)	AW3D30 (30m)	Open	2.60	2.13
		Forest	4.14	3.10
		Water	3.47	2.66

The frequency distributions of height differences between GDEMs are given in Figures 6 and 7 for inclined and uninclined areas. NMAD is continuously smaller than SZ both in Figures 6 and 7 and the distributions are symmetric which indicate normal distribution. Another positive is the peaks of height differences which are around zero that means full coherence. The most important outcome is ±12 m limit of height differences which demonstrate the minor level of outliers. Stated in other words, all of the pixels in GDEMs have ≤12 m height difference which can be claimed a good coherence for space-borne data.

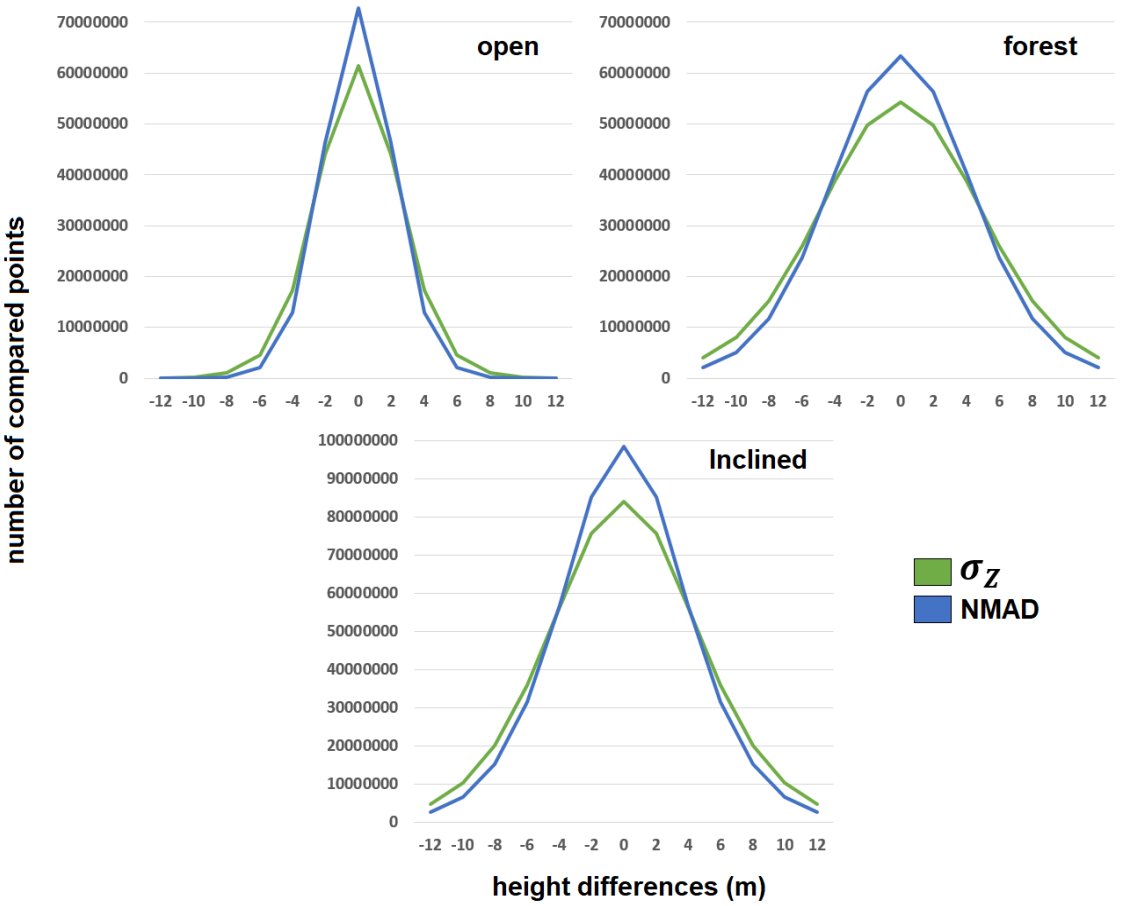

Figure 6. Frequency distribution of height differences based on SZ and NMAD

6

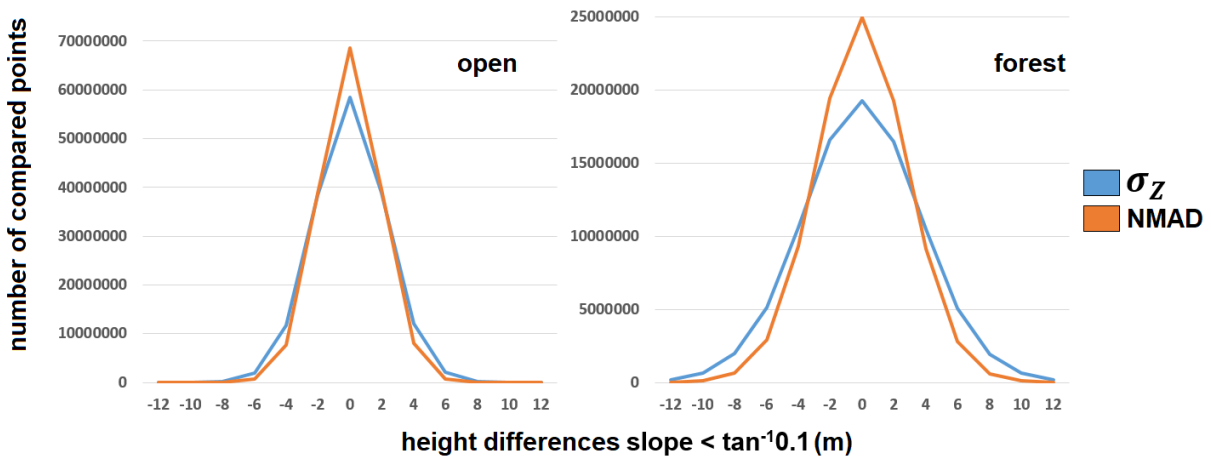

Figure 7. Frequency distribution of height differences based on SZ and NMAD in uninclined parts (slope < $\tan^{-1}0.1$)

Figure 8 shows the coherence map of SRTM and AW3D30 GDEM on Turkey. Generated coherence map exhibits the problems of GDEMs in inclined and forest regions. In the map, the scale of coherent and incoherent parts is presented again by ±12 m. Almost all of incoherent regions are located in the steep and the dense forests of the stu8dy area.

If the coherence map is examined in detail, the inverse coherence in sequential vertical lines can be noticed. In contrast to optical imaging, SAR acquires space-borne data using ascending (south to north) and descending (north to south) passes in near-polar orbits. In ascending and descending passes, amount of acquired data is different depending on sun-light and darkness. In darkness, the solar panels cannot generate power that's why more data is acquired in sun-light. The coherence map demonstrates the effect of ascending and descending orbits on the topographic description potential of SAR data clearly. Line by line, the height differences between SRTM and AW3D30 GDEMs reverse as blue tones and turquoise tones.

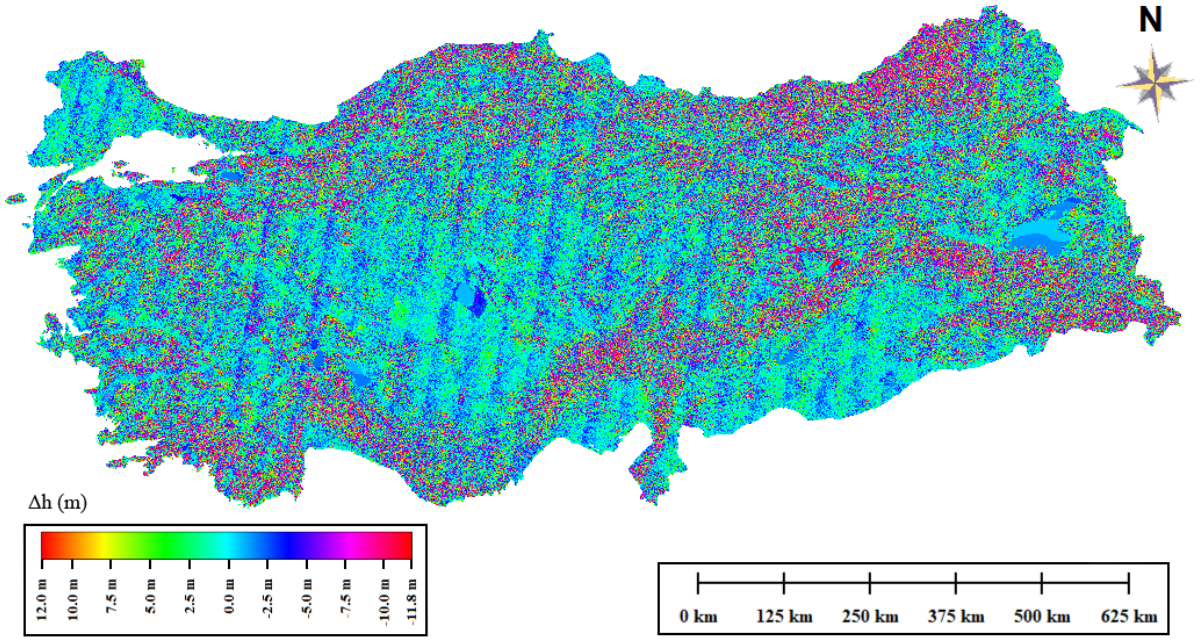

Figure 8. Coherence map of SRTM and AW3D30 GDEMs

In Figure 8, the most problematic parts are mountainous and forest covered regions (Please check Figure 4 for land cover classification). The most important cause for low coherence between ALOS and SRTM GDEMs is the spatial resolution of the data used for the generation of these GDEMs. The AW3D30 GDEM was generated from ALOS Prism imagery which have 2.5 m ground sampling distance (GSD) while SRTM GDEM has derived from 30 m × 20

7

m (azimuth × range) C-band SAR imagery. Due to this fact, topographic description of AW3D30 is closer to the real surface in comparison with SRTM C-band GDEM (Sefercik et al. 2018).

Conclusions

In this study, coherence between 1 arc-second gridded SRTM and AW3D30 GDEMs were investigated by visual and quantitative analysis in country scale. Regarding the challenges of space-borne remote sensing imaging geometries, the study area which have a mountainous topography and dense forest coverage was preferred. In this manner, coherence between GDEMs in hard conditions was investigated. The results demonstrated that the coherence of SRTM and AW3D30 is ≤ 1 pixel (30 m) in horizontal direction and ± 12 m in height. The influence of land cover and terrain inclination was visualized by error distribution graphics and coherence maps. In the frequency distribution of height differences graphics, a normal and symmetric distribution were specified. Effect of ascending and descending flying orbits (aspects) on SAR imaging was clearly demonstrated.

Overall, in open and flat areas, the coherence of SRTM and AW3D30 GDEMs are high as expected. However, in forest and inclined regions, scientific and commercial users should be very careful in preferring the correct GDEM. Although freely available in equal grid spacing, the topographic description potentials are different due to 2.5 m GSD ALOS Prism and 30 m × 20 m C-band images which are used for GDEM generation.

ACKNOWLEDGEMENTS

We would like to thank NASA and JAXA for freely supporting 1 arc-second SRTM C-band and AW3D30 GDEMs.

REFERENCES

Alobeid, A., Jacobsen, K., Heipke, C., 2010. Comparison of Matching Algorithms for DSM generation in urban areas from IKONOS imagery. Photogrammetric Engineering & Remote Sensing, 76(9):1041–1050.

Baltsavias, E., Gruen, A., Eisenbeiss, H., Zhang, L., Waser, T., 2008. High-quality image matching and automated generation of 3D tree models. International Journal of Remote Sensing 29(5):1243–1259.

Bullard, J. E., White, K., Livingstone, I., 2011. Morphometric analysis of aeolian bedforms in the Namib Sand Sea using ASTER data. Earth Surface Processes and Landforms, 36(11):1534–1549.

Carvalho, O., Guimaraes, R., Freitas, L., 2010. Urbanization impacts upon catchment hydrology and gully development using mutli-temporal digital elevation data analysis. Earth Surface Processes and Landforms, 35(5):611–617.

Cuartero, A., Felicisimo, A. M., Ariza, F. J., 2005. Accuracy, reliability, and depuration of SPOT HRV and Terra ASTER digital elevation models. IEEE Transactions on Geoscience and Remote Sensing, 43(2):404–407.

DeLong, S. B., Prentice, C. S., Hilley, G. E., Ebert, Y., 2012. Multitemporal ALSM change detection, sediment delivery, and process mapping at an active earthflow. Earth Surface Processes and Landforms, 37(3):262–272.

Heckmann, T., Bimbose, M., Krautblatter, M., Haus, F., Becht, M., Morshe, D., 2012. From geotechnical analysis to quantification and modelling using Li-DAR data: A study on rockfall in the Reintal catchment, Bavarian Alps, Germany. Earth Surface Processes and Landforms, 37(1):119–133.

Hellerstein, J. M., 2008. Quantitative Data Cleaning for Large Databases. Technical Report Presented at United Nations Economic Commission for Europe (UNECE), p. 42.

Hobi, M. L., Ginzler, C., 2012. Accuracy assessment of digital surface models based on WorldView-2 and ADS80 stereo remote sensing data. Sensors, 12(5): 6347–6368.

Li, R., Zhou, G., Schmidt, N. J., Fowler, C., Tuell, G., 2002. Photogrammetric processing of high-resolution airborne and satellite linear array stereo images for mapping applications. International Journal of Remote Sensing, 23(20):4451−4473.

Radhadevi, P. V., Solanki, S. S., Nagasubramanian, V., Mahapatra, A., Sudheer, R. D., Jyothi, M. V., Krishna, S., Saibaba, J., Geeta, V., 2010. New era of Cartosat satellites for large scale mapping. Photogrammetric Engineering and Remote Sensing, 76(9):1031−1039.

Schneider, A., Gerke, H. H., Maurer, T., Seifert, S., Nenov, R., Hüttl, R. F., 2012. Evaluation of remotely-sensed DEMs and modification based on plausibility rules and initial sediment budgets of an artificially-created catchment. Earth Surface Processes and Landforms, 37(7):708−725.

Sefercik, U. G., Soergel, U., 2010. Comparison of High Resolution InSAR and Optical DEMs. EARSeL Joint SIG Workshop, Ghent. (on CDROM).

Sefercik, U. G., Buyuksalih, G., Atalay, C., Jacobsen, K., 2018. Validation of Sentinel-1A And AW3D30 DSMs for the Metropolitan Area of Istanbul, Turkey, Journal of Photogrammetry, Remote Sensing and Geoinformation Science, 86(3-4): 141-155.

Soergel, U., Michaelsen, E., Thiele, A., Cadario, E., Thoennessen, U., 2009. Stereo analysis of high-resolution SAR images for building height estimation in case of orthogonal aspect directions. ISPRS Journal of Photogrammetry and Remote Sensing, 64(5):490−500.

Toutin, T., 2008. ASTER DEMs for geomatic and geoscientific applications: A review. International Journal of Remote Sensing, 29(7):1855−1875.

9